IMAGE RECONSTRUCTION STRATEGIES USING DUAL MODALITY MRI-NIR DATA

Hamid Dehghani[1,2], Brian W. Pogue[1], Ben Brooksby[1], Subhadra Srinivasan[1], and Keith D. Paulsen[1]*

[1]Thayer School of Engineering, Dartmouth College, Hanover, NH 03755, USA
[2]School of Physics, University of Exeter, Exeter EX4 4QL, UK
* email: h.dehghani@exeter.ac.uk

ABSTRACT

An imaging system which simultaneously performs near infrared (NIR) tomography and magnetic resonance imaging (MRI) has been developed at Dartmouth College, to study breast tissue of women *in vivo*. A NIR image reconstruction technique which exploits the combined multi-wavelength data set is presented which implements the MR structure as a soft-constraint in the NIR property estimation. The benefits of spatial and spectral priors, applied independently and together, in NIR diffuse tomography image reconstruction of *in vivo* measurements are presented. When both spatial and spectral priors are applied in a healthy volunteer, glandular tissue shows higher total blood content, water, and scattering power compared to fatty tissue.

1. INTRODUCTION

Near Infrared (NIR) optical tomography is a non-invasive imaging technique that aims to reconstruct images of tissue function and physiology, specifically in this study, for the detection and characterization of breast cancer [1-3]. The advantages of NIR breast imaging over conventional imaging techniques, such as X-ray mammography, include the use of non-ionizing radiation which permits continuous monitoring of subjects, as well as the unique spectral signature of biological tissue with respect to the wavelength of the applied NIR signal. Typically, light is applied to the surface of the tissue, in this case the breast, by the use of optical fibers, and the measured intensity and path-length of the out-coming light from other surface mounted fibers are used, together with a model based reconstruction algorithm to produce images of the internal light attenuation μ_a and reduced scatter μ_s' coefficient distribution.

This work explores the combination of structural and functional imaging into a single platform for the study of breast tissue. Functionally, NIR contrast mechanisms in tissue are dominated by elastic Mie-like scattering. Measured signals are highly sensitive to tissue concentrations of oxyhemoglobin, deoxyhemoglobin, and water. Structurally, contrast in MRI derives from intrinsic tissue factors related to micromagnetic structural inhomogeneities. Relaxation times vary substantially for different tissues and are strongly dependent on their physical characteristics.

In addition to co-registration, data sets from combined NIR and MRI imaging offer other synergistic benefits, namely anatomical priors (from high spatial resolution MRI) enhance NIR (i.e. high contrast resolution) image reconstruction. NIR spectroscopy is biochemically rich, but spectroscopic imaging is hindered by the highly scattered photon paths that reduce resolution in tissue. The most widely adopted approach to this problem incorporates parameter estimation strategies based on models of light propagation in tissue. The estimation task is sensitive to small perturbations in the light measurements, not all of which are caused by the intrinsic changes in tissue optical properties. Experience has shown that significant improvement in the stability and accuracy of the reconstruction process can be obtained by including prior anatomical/optical information [4]

Studies have shown that anatomical information from other modalities such as MRI or ultrasound, when used in the reconstruction procedure, can improve the stability of the reconstruction and result in faster convergence [5] [6] [7]. Brooksby et al [4] explored a method for encoding MRI priors into a spatially varying regularization, thereby eliminating the requirement that spatial constraints be exact. In that study, phantom data at a single wavelength was used to show that quantitative accuracy and spatial resolution of optical property images could be improved without increasing vulnerability to systematic errors. While most studies have shown that resolution, stability and convergence can be improved by use of anatomical information from another high-resolution imaging modality, it is still unclear how this improves the quantitative spectroscopic accuracy.

The other prior that can be applied is from NIR tomography itself—the use of the spectral behavior of tissue chromophores and Mie theory approximation for scattering as constraints. This type of reconstruction uses multi-wavelength measurements simultaneously and recovers the images of oxyhemoglobin, de-oxyhemoglobin, water and scatter parameters directly, without intermediate recovery of optical properties. This type of parameter reduction makes the problem less under-determined, and significantly

reduces the crosstalk between various parameters. Corlu et al [8] and Li et al [9] applied this technique to continuous-wave data, with suitable assumptions regarding scatter, and showed optimized images with lower cross-talk in simulations. Srinivasan et al [10] have extended this approach to frequency domain, and showed experimental evidence of improved quantification.

In this abstract, we compare the approach of spectral priors to spatial priors applied to clinical data, and show that the use of the two priors together may be the solution to obtaining images that are quantitatively accurate and qualitatively superior.

2. METHOD

2.1 Instrumentation

The imaging system used records measurements of NIR light transmission through a pendant breast in a planar, tomographic geometry. The patient lies inside a 1.5 T whole body MRI (GE Medical Systems) and the two data types (i.e. NIR and MRI) are acquired simultaneously. The system is shown in Figure. 1, and has been described in detail by Brooksby et al. [6]. Figure 1(a) shows the portable cart which contains the light generation and detection hardware subsystems. Six laser diodes (660-850 nm) are amplitude modulated at 100 MHz. The bank of laser tubes is mounted on a linear translation stage, which sequentially couples the activated source into 16 bifurcated optical fiber bundles. The central fibers deliver the source light while the remaining fibers collect transmitted light and are coupled to photomultiplier tube (PMT) detectors located in the base of the cart. The fibers are positioned in a plane spanning the circumference of a pendant breast, and for each activated source, measurements of the amplitude and

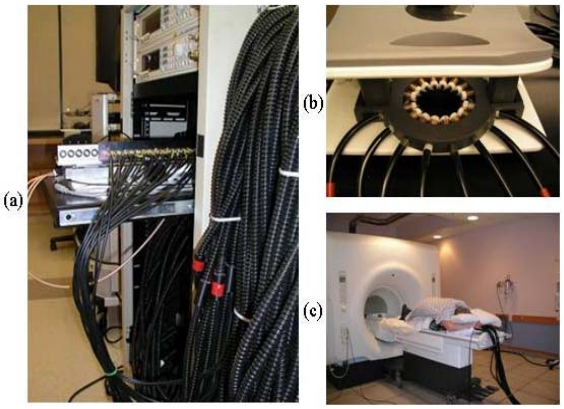

Figure 1. Photograph of the portable cart housing the NIR light generation and detection hardware. The cart stands outside of the RF shielded MR chamber, and optical fibers extend 13 meters to the MRI patient bed.

phase shift of the 100 MHz signal are acquired from 15 locations around the breast. Figure 1(b) shows a photograph of the MR-compatible fiber positioning system anchored inside an open architecture breast array coil (MRI Devices). The vertical position of the imaging plane is manually adjusted, and contact with the breast is maintained

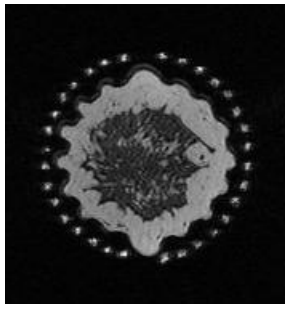

Figure 2. The anatomically coronal MRI of the breast of a normal female volunteer who was imaged with our simultaneous NIR-MRI imaging system. Optical fibers surround the breast perimeter, their location indicated by fiducial markers in the MRI. Two tissue types are visible: adipose tissue appears light gray, and composes an outer layer which surrounds the darker area of fibroglandular tissue.

automatically using bronze compression springs.

2.2 Image Reconstruction

The inverse problem being ill-posed, as often is the approach, we seek to minimize the least squares functional

$$\chi^2 = \sum_{j=1}^{M} \left(\phi_j^m - \phi_j^c \right)^2 \qquad (1)$$

where M is the total number of measurements at each wavelength, and ϕ_j^m and ϕ_j^c are the measured and calculated fluence at the boundary for each measurement point j. The minimization in Equation (1) is carried out by applying a Newton-Raphson iterative method where the boundary data is calculated at a sufficiently close set of initial optical properties, along with the Levenberg Marquardt regularization for stabilizing the inversion. The inversion is given by the matrix equation

$$\partial\mu = \left(J^T J + \alpha I \right)^{-1} J^T \partial\phi \qquad (2)$$

where J is the Jacobian containing the derivatives of ϕ with respect to the optical properties μ given by (μ_a, κ), where μ_a is the absorption coefficient in mm^{-1} and κ is the diffusion coefficient ($\kappa = 1/3(\mu_a + \mu_s')$ in mm), and μ_s' is the reduced scattering coefficient in mm^{-1}. α governs the regularization or smoothness applied to the problem which balances data errors due to noise. Solving Equation (2) using $\partial\phi = \left(\phi^m - \phi_k{}^c \right)$, we obtain a new search direction for the solution for the k^{th} iteration μ_k from $\delta\mu$, our measure of convergence being χ^2 less than 2% of that of the previous iteration.

Solving the inverse problem in this manner, absorption and reduced scattering coefficient images at six

wavelengths are obtained and this is followed by a least squares fit to Beer's law, $\mu_a = [\varepsilon]c$, where ε is the molar absorption spectra of the absorbing tissue chromophores, in our case, oxy-hemoglobin (HbO_2), deoxy-hemoglobin (Hb), and water, and c is their concentrations (dimensions of $3 \times N$, where N = number of unknowns within the model, i.e. nodes). Similarly, for scattering the approximation to Mie theory $\mu_s' = A\lambda^{-b}$ is used to derive images of scatter amplitude (A) and scatter power (b), where λ is the wavelength in microns. Both variables A and b are vectors of length $N \times 1$.

In order to implement these spectral relationships into the reconstruction directly, the least squares functional is modified to be

$$\chi^2 = \sum_{j=1}^{Mn} \left(\phi_j^m - \phi_j^c\right)^2 \qquad (3)$$

so that j now includes all wavelength measurements (Mn), where n is the number of wavelengths available (6 in our case). The Newton method then gives a different relationship, which for each wavelength is represented by

$$\partial\phi_\lambda = J_{c,\lambda}\delta c + J_{A,\lambda}\delta A + J_{b,\lambda}\delta b \qquad (4)$$

where $J_{c,\lambda}$, $J_{A,\lambda}$ and $J_{b,\lambda}$ represent the Jacobians for each of the chromophore and scattering parameters. The relationships between these Jacobians and $J_{\mu_a} = \frac{\partial\phi}{\partial\mu_a}$ and $J_\kappa = \frac{\partial\phi}{\partial\kappa}$ calculated before have been derived in [10] and Equation (2) is suitably modified so that the update in chromophores ∂c occurs directly:

$$\partial c = \left(\tilde{J}^T\tilde{J} + \alpha I\right)^{-1}\tilde{J}^T\partial\phi \qquad (5)$$

where

$$\partial\phi = \left(\phi^{m,\lambda} - \phi_k^{c,\lambda}\right)_{\lambda=1:n} \qquad (6)$$

and

$$\tilde{J} = \left[J_{c,\lambda}, J_{A,\lambda}, J_{b,\lambda}\right]_{\lambda=1:n} \qquad (7)$$

In order to add the spatial constraint to this further, the minimization functional is modified to include a penalty term for *a priori* information of tissue structure, given by:

$$\chi^2 = \sum_{j=1}^{Mn}\left(\phi_j^m - \phi_j^c\right)^2 + \beta\sum_{j=1}^{Mn} L(\mu_j - \mu_{o,j})^2 \qquad (8)$$

where β is the regularizing term for spatial prior and L is a matrix generated using MRI-derived spatial information, acting on the solution μ. This matrix links all the nodes in a particular type tissue (glandular or fatty) so that a second differential operator is approximated within each region. This is similar to total variation minimization approach allowing sharp boundaries to exist, while providing flexibility to encode these boundaries from MRI information. Each node in the FEM mesh is labeled according to the region, or tissue type, with which it is associated (in the MR image). For the i^{th} node in region R, $L_{i,i}=1$. When nodes i and j are in the same region, $L_{i,j}= -1/n$, where n is the total number nodes within region R, otherwise $L_{i,j}=0$. Applied with the spectral prior, the final matrix equation is

$$\partial c = \left(\tilde{J}^T\tilde{J} + \alpha I + \beta L^T L\right)^{-1}\tilde{J}^T\partial\phi \qquad (9)$$

The values for α, β have been chosen empirically to be 10 through simulations and experiments.

2.3 Data Collection

The combined NIR-MRI imaging system described above was used in a case study to estimate the properties of healthy breast tissue. A FEM mesh generated from the MRI of the healthy female volunteer shown in Figure 2 was used in the reconstruction. The locations (nodes) of this mesh are each associated with grayscale intensity in the co-registered MRI, and are classified as representing either glandular or adipose tissue. Figure 3 shows the tissue properties estimated with the four procedures used which are (I) Assuming no a-priori information, except the outer bounder of the breast as obtained from the MRI image shown in Figure 2, (II) a spatially constrained reconstruction algorithm, whereby a "Laplacian Type" penalty function is used to associate nodes of each specific region of glandular or fatty tissue together, (III) A spectrally constrained reconstruction algorithm, whereby the data from all wavelengths are used simultaneously to calculate images of total hemoglobin (Hb_T), oxygen saturation (S_tO_2), water concentration (H_2O), scattering amplitude (A) and power (b), (IV) Both a spectral and spatial constrains are applied simultaneously.

3. RESULTS

The images obtained for the NIR parameters using an unconstrained reconstruction shows (Figure 3) noisy images with boundary artifacts. The spatial priors act on these images, making them smoother, but preserving the trend for the quantification. For example, the scatter power shows a reduction in the glandular tissue (row 2) similar to the values obtained in the no-priors reconstruction (row 1). However, previous studies have indicated that, glandular tissue having higher number density of scatterers, may actually have higher values for scatter power, than fatty tissue. Hence, the results from spatially constrained reconstruction, while appearing smoother, may be misleading. The scatter power image obtained by application of the spectrally constrained method is more

quantitatively acceptable and the spatial priors acting on this spectral method gives the most intuitively acceptable image for this parameter, showing the layered structure of the

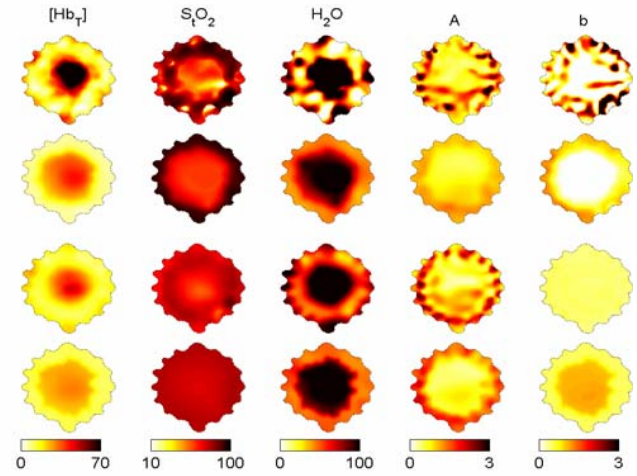

Figure 3. Breast tissue property images for a healthy female volunteer estimated using four different reconstruction methods. First (top), only the outer boundary of the imaging domain, and the location of the optical fibre measurement sites are specified. Second, a spatially constrained algorithm was used. The MRI of this patient defined the spatial constraints, which relate to the internal distribution of adipose and glandular tissues. Third, spectral constraints were applied and chromophore concentrations and scattering parameters were reconstructed directly. Fourth (bottom), both spatial and spectral constraints were combined.

breast tissue. We observed elevated [Hb_T] (25:13 μM), water (91:49 %), and scattering power (1.0:0.5) in glandular tissue relative to adipose tissue using the combined priors, which matches the higher vascularization in the glandular tissue.

4. DISCUSSION

Our results presented here show that, while anatomical information improves the image quality resulting in reduced artifacts, it may not significantly improve quantification. The spectral prior obtained using the intrinsic behavior of tissue chromophores and scattering in the near infrared wavelength regime plays a more important role in addressing this problem, and finally, a synergy between these two priors yields the most accurate characterization of breast tissue properties currently possible.

5. ACKNOWLEDGEMENTS

This work has been funded by NIH research grants RO1CA69544, PO1CA80139, and U54CA105480, and by the DOD breast cancer research program, DAMD17-03-1-0405.

6. REFERENCES

1. Dehghani, H., et al., *Multiwavelength Three-Dimensional Near-Infrared Tomography of the Breast: Initial Simulation, Phantom, and Clinical Results.* Applied Optics, 2003. **42**(1): p. 135-145.
2. Gibson, A., Hebden, JC, and Arridge, SR, *Recent advances in diffuse optical imaging.* Phys. Med. Biol., 2005. **50**: p. R1-R43.
3. Poplack, S.P., Paulsen, K. D., Hartov, A., Meaney, P. M., Pogue, B. W., Tosteson, Tor D., Grove, M. R., Soho, S. K., and Wells, W. A., *Electromagnetic Breast Imaging: Average Tissue Property Values in Women with Negative Clinical Findings.* Radiology, 2004. **231**: p. 571-580.
4. Brooksby, B., Jiang, S., Dehghani, H., Pogue, B. W., Paulsen, K. D., Weaver, J., Kogel, C., and Poplack, S. P., *Combining near infrared tomography and magnetic resonance imaging to study in vivo breast tissue: implementation of a Laplacian-type regularization to incorporate magentic reasonance structure.* JBO, 2005. **10**(5).
5. Arridge, S.R. and M. Schweiger, *Sensitivity to prior knowledge in optical tomographic resconstruction.* Proc. SPIE, 1995. **2389**: p. 378-388.
6. Brooksby, B., et al., *Magnetic Resonance-Guided Near-Infrared Tomography of the Breast.* Rev. Sci. Instrum., 2004. **75**(12).
7. Ntziachristos, V., X.H. Ma, and B. Chance, *Time-correlated single photon counting imager for simultaneous magnetic resonance and near-infrared mammography.* Review of Scientific Instruments, 1998. **69**(12): p. 4221-4233.
8. Corlu, A., et al., *Diffuse optical tomography with spectral constraints and wavelength optimization.* Appl. Opt., 2005. **44**(11): p. 2082-2093.
9. Li, A., et al., *Reconstructing chromosphere concentration images directly by continuous-wave diffuse optical tomography.* Opt. Lett., 2004. **29**(3): p. 256-258.
10. Srinivasan, S., Pogue, B. W., Jiang, S., Dehghani, H., and Paulsen, K. D., *Spectrally Constrained Chromophore and Scattering NIR Tomography Provides Quantitative and Robust Reconstruction.* Appl. Opt., 2005. **44**(10): p. 1858-1869.